SAND99-1810C

GAS PHASE CHEMICAL DETECTION WITH AN INTEGRATED CHEMICAL ANALYSIS SYSTEM

Stephen A. Casalnuovo, Gregory C. Frye-Mason, Richard J. Kottenstette, Edwin J. Heller, Carolyn M. Matzke, Patrick R. Lewis, Ronald P. Manginell, Albert G. Baca, Susan L. Hietala, W. Kent Schubert, Vincent M. Hietala, Darryl Y. Sasaki, and John L. Reno

Sandia National Laboratories
P. O. Box 5800, MS-1425
Albuquerque, NM, USA 87185-1425

ABSTRACT

Microfabrication technology has been applied to the development of a miniature, multi-channel gas phase chemical laboratory that provides fast response, small size, and enhanced versatility and chemical discrimination. Each analysis channel includes a sample concentrator followed by a gas chromatographic separator and a chemically selective surface acoustic wave detector array to achieve high sensitivity and selectivity. The performance of the components, individually and collectively, is described. The design and performance of novel micromachined acoustic wave devices, with the potential for improved chemical sensitivity, are also described.

1. INTRODUCTION

Numerous chemical detection scenarios, for example, industrial process control and public safety applications, impose challenging requirements on the performance of chemical detection systems. These applications require detection of trace levels of specific target analytes in real-world environments that may contain more than 1000-fold higher concentrations of potentially interfering compounds. In addition, rapid analysis, instrument portability, and low rates of compound misidentification often are critically important. In an effort to address the requirements of these applications, Sandia's μChemLab™ program has a goal to develop small (palm-top computer sized), lightweight, and autonomous systems that provide rapid (1 min), sensitive (1-10 parts per billion (ppb)), and selective detection of target analytes. Although the μChemLab™ program includes gas and liquid phase analysis systems, only the performance of the gas phase components, being optimized for chemical warfare (CW) agent detection, is described herein.

Figure 1 shows the system design utilizing multiple analysis channels to provide enhanced chemical discrimination and very low false alarm rates. Sensitive and highly selective detection is achieved using a small adsorbent sample concentrator connected to a gas chromatographic (GC) column that feeds a low dead volume surface acoustic wave (SAW) detector array. Commercially available batch microfabrication processes are employed to produce these three components, pictured in Fig. 2. Among the advantages of this approach are size and cost minimization for individual devices. The design and performance of the current component set is described below, along with the development of novel, potentially more sensitive, acoustic wave chemical sensors.

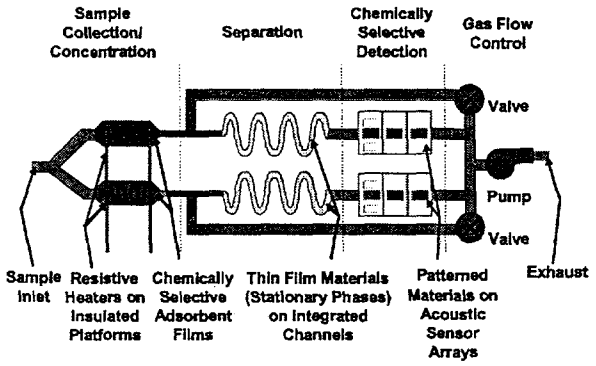

Fig. 1: Schematic of the gas-phase μChemLab™ system. The system incorporates Sandia designed and fabricated concentration, separation, and detection components (see Fig. 2) and commercially available diaphragm pumps and miniature valves.

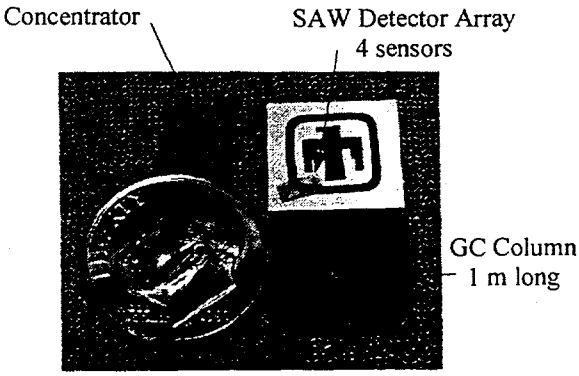

Fig. 2: Clockwise from above U.S. dime used for scale (18 mm diameter): microfabricated sample concentrator; four-element, 380 MHz SAW detector array, and 1 m long gas chromatograph column.

DISCLAIMER

2. CONCENTRATOR

The concentrator stage collects target analytes from the air stream over an extended time and then releases them in a rapid, concentrated pulse into the GC column. This device, in essence, is a microfabricated hotplate (see Figs. 3 and 4). A chemically selective layer, typically a microporous oxide, adsorbs the analytes from the environment. After sufficient analyte has been collected, an embedded Pt heater rapidly raises the temperature of the concentrator to desorb the analytes. Concentration enhancement factors of greater than 100 have been achieved after 40 s adsorption periods. The desorption pulse width is 200 ms (full width at half maximum).

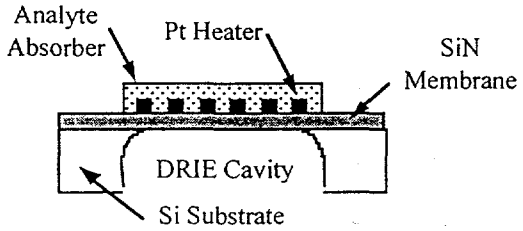

Fig. 3: Schematic cross section of the microhotplate concentrator stage.

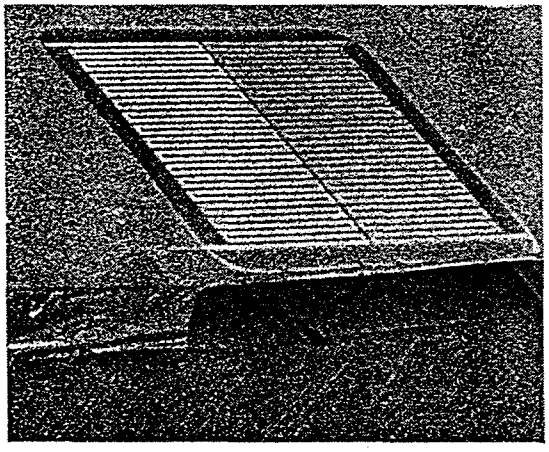

Fig. 4: Scanning electron micrograph (SEM) of the concentrator stage showing the micromachined SiN membrane and Pt heater. Analyte adsorbing layer is not shown.

The heater is fabricated on a 0.5 μm thick silicon nitride (SiN) membrane suspended over a cavity etched through a Si substrate. The 400 μm deep cavity is produced using deep reactive ion etching (DRIE) [1]. The low thermal mass and good thermal isolation of the SiN membrane are critical for quickly heating the concentrator with a minimum of electric power. As shown in Fig. 5, the microhotplate requires approximately 20 ms to reach a steady-state temperature of 200°C. This steady-state temperature is sustained by 105 mW of electrical power. Thermal modeling has been used to optimize the concentrator design [2].

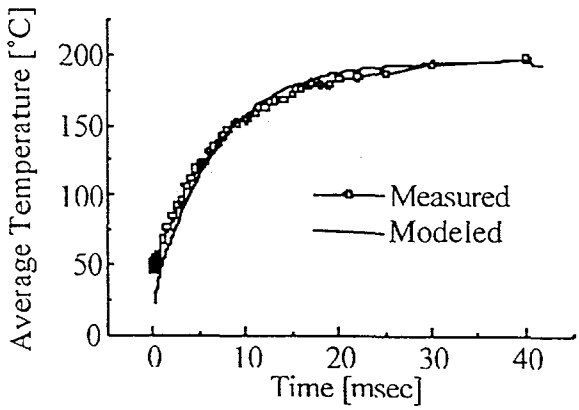

Fig. 5: Comparison of measured and modeled heating rates of the microhotplate concentrator during analyte desorption. The concentrator can be ramped from room temperature to 200°C in 20 ms, drawing 105 mW at steady-state.

For prototype testing, the concentrator is mounted in a standard integrated circuit package that provides the electrical interconnections. A glass lid with machined gas flow channels is glued directly to the Si concentrator substrate. Microcapillary tubes are inserted into through holes machined in this lid to provide interconnection to a miniature pump, valve, and the GC column.

3. GC COLUMN

A miniature GC column provides temporal separation of the analytes and any interferants that may pass through the concentrator stage. A Si DRIE process, similar to that used to fabricate the concentrator, is employed to produce the GC column [3]. Because of the exceptionally high aspect ratio and anisotropy of the DRIE process, closely spaced, narrow gas flow channels can be etched into the Si substrate to a depth many times the channel width. This approach affords good GC performance in a small footprint while maintaining short transit times through the column. A typical column is a 1 m long spiral with 40 μm wide channels separated by 40 μm thick walls etched to a depth of 300 μm (see Fig. 2). It occupies a 1 cm^2 area. The close-up of a channel cross-section in Fig. 6 illustrates the capability of the fabrication process. After the channels are etched, the Si substrate is thermally oxidized to produce a thin, glasslike layer on the surface of the channels in order to facilitate stationary phase deposition (see below).

Closed channels are produced by anodically bonding a Pyrex lid to the top surface of the Si substrate [3]. Since the bonding process is carried out at elevated temperatures, Pyrex is used because it closely matches Si's thermal expansion coefficient.

As with the concentrator, microcapillary tubes are inserted into through holes machined in this lid to provide gas interconnection.

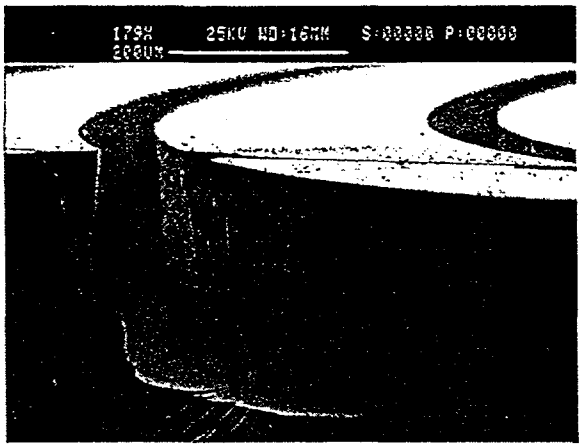

Fig. 6: SEM of a cross-section of a spiral GC column etched into Si using DRIE. The etch process results in deep, smooth, vertical channels.

After the channels are sealed, GC stationary phase materials are deposited on the walls using conventional polymer solution techniques as well as sol-gel coating technology. The retention of the analytes in the stationary phase produces a separation in time of the analytes arriving at the array of acoustic wave detectors. This temporal separation provides an additional means of distinguishing analytes from one another and from interferants, as shown in Fig. 7, aiding in analyte identification.

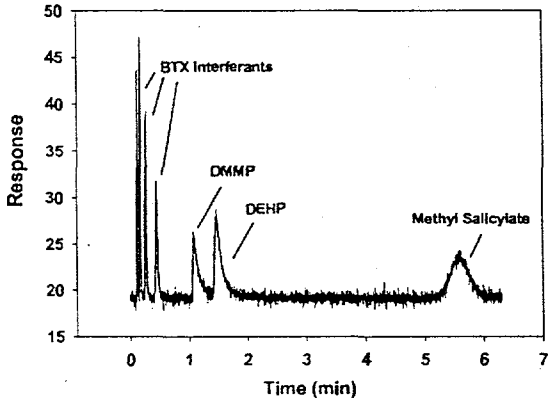

Fig. 7: Microfabricated GC column elution times for a mixture of dimethylmethylphosphonate (DMMP), diethylhydrogenphosphate (DEHP), methyl salicylate, all simulants for CW agents, and benzene (B), toluene (T), and xylene (X), interferants present in gasoline vapor.

As illustrated in Fig. 1, the μChemLab™ system will have two gas analysis channels that incorporate GC columns, each with a different stationary phase. The two channels can be optimized for different analytes, increasing the functional range of the unit. The channels can also be optimized to provide two analyses for an analyte, improving the reliability and lowering the false alarm rate, as demonstrated in Fig. 8. The stationary phase selection, in this case, non-polar versus polar, reorders the elution times of the components.

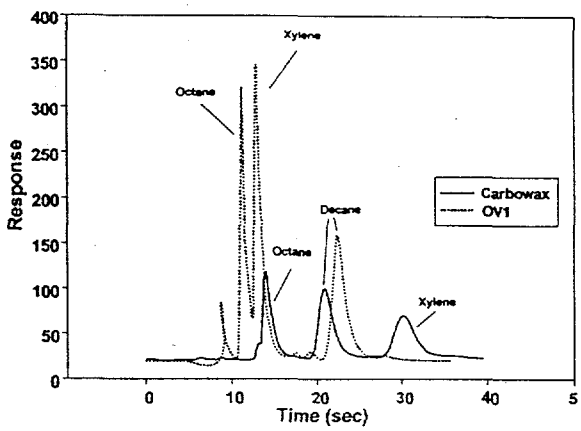

Fig. 8: Elution times for two microfabricated GC columns with different stationary phases (Carbowax and OV1). Reordering of elution times in the two channels provides confirmation of results.

4. SAW CHEMICAL SENSOR ARRAY

The use of SAW delay lines as sensitive chemical mass sensors is well known [4]. The μChemLab™ employs a 4-element quartz array in each gas analysis channel, as shown in Fig. 9. A center input interdigitated transducer (IDT) launches a SAW in both directions. Four smaller output IDTs, two on either side of the input IDT, reconvert the acoustic wave to an electric signal. Three of the SAW delay lines are coated with different chemically sorbent materials, each optimized for the analytes of interest. The fourth delay line serves as a reference. Delay lines operating between 100 MHz and 700 MHz have been designed and tested. Delay line frequency is determined by the spacing between adjacent IDT fingers and the acoustic velocity in the material.

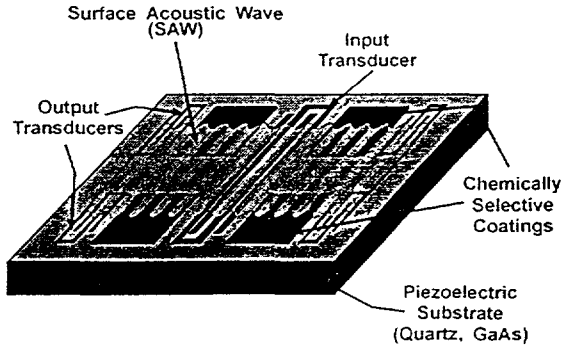

Fig. 9: Schematic representation of a 4-element SAW detector array.

The delay line frequency is a critical parameter in the design and operation of the SAW sensor array. When a delay line is configured in an oscillator circuit, the sensitivity of the oscillator frequency, f, to added surface mass density (mass/area) increases as f^2 [4]. In addition, the size of the delay line decreases as $1/f^2$. The net result is that the sensitivity to the total mass of the analyte scales as f^4, which is a strong argument for going to higher frequency. These trends are illustrated in Fig. 10. The scaling of the detection limit for a delay line sensor, that is, the smallest amount of added mass that can be detected, depends on how the system noise scales with frequency. The frequency dependence of sensor noise is currently being studied.

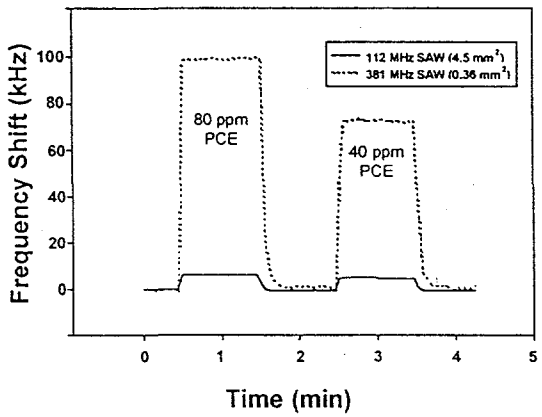

Fig. 10: Sensitivity data for two SAW devices with identical coatings when exposed to perchloroethylene vapors. The higher frequency SAW is much smaller, but exhibits a much larger response.

All three microfabricated components, the concentrator, GC column, and SAW detector array, have been assembled in a laboratory test system to evaluate their collective performance. An example of the system performance, showing the temporal separation of target analytes and the varied response of the three elements in the SAW detector array, is given in Fig. 11. The initial gas sample contained DMMP and DHEP at a concentration of 100 ppb. Analyte gas flowed over the concentrator for 3 minutes prior to thermal desorption. SAW response was measured with a phase demodulation technique.

Within the actual prototype unit, the SAW sensor array is driven by custom, high frequency GaAs integrated circuits (IC). The reference delay line is wired into the feedback path of an IC amplifier. The phase delay of each of the three sensor delay lines is compared to the reference by an IC phase comparator. This IC produces a DC voltage proportional to the phase difference between the sensor delay line and the reference delay line. As analytes are sorbed by the coatings on the three sensor delay lines, the added surface mass decreases the velocity of the SAW, producing a change in phase in the delay line. With this approach, sub-picogram detection limits are possible.

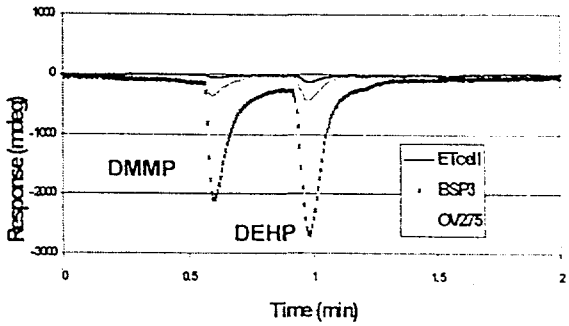

Fig. 11: SAW sensor array response to mixture of DMMP and DEHP after passing through the concentrator and GC column. Sensor array elements were coated with ethyl cellulose (Etcell), a H-bond acid modified polymer (BSP3) [5], and a cyano-modified polysiloxane (OV275).

The attraction of higher frequency SAW sensors is reduced somewhat by the difficulty associated with packaging high frequency components. This problem is minimized if all high frequency components, including the SAW delay line, can be monolithically integrated onto a single IC requiring only DC electrical power as input and providing a DC output. As a first step in this approach, we have integrated a high frequency amplifier and a single SAW delay line onto a GaAs substrate [6] (Fig. 12). This is possible because GaAs is both semiconducting and piezoelectric. This oscillator circuit requires only a 3.5 VDC power supply to operate. Frequency response for the integrated oscillator is shown in Fig. 13. While this circuit requires only a DC input, it still yields a high frequency output. The next step in this development is to integrate a second delay line and the phase comparator circuit for complete DC in/DC out, single chip operation. This effort is currently underway.

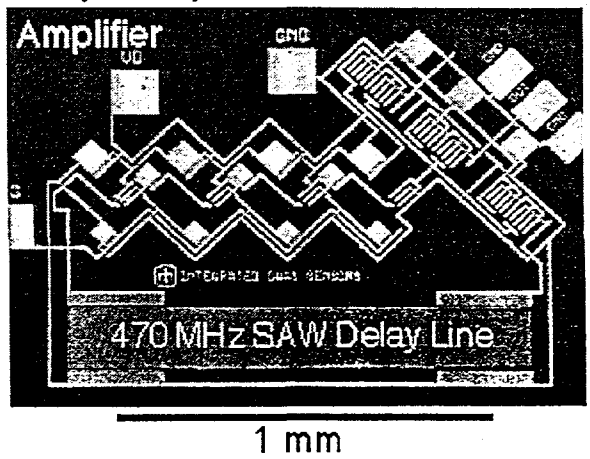

Fig. 12: Micrograph of an integrated GaAs SAW delay line oscillator with a SAW delay line in the feedback loop of a high frequency amplifier. The oscillator operates at 470 MHz.

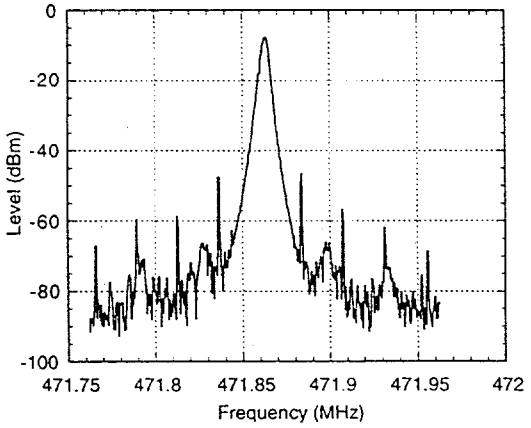

Fig. 13: Frequency response of integrated GaAs oscillator shown in Fig. 12

5. ACOUSTIC WAVE DEVICE DEVELOPMENT

As a sensor material, GaAs has advantages beyond the integration of acoustic wave transducer and microelectronics. With the application of micromachining processes analogous to those found in Si micro-electro-mechanical systems (MEMS) technology, it is possible to produce freely suspended GaAs membranes that retain all the crystalline properties of bulk GaAs [7]. We have used this approach to fabricate acoustic wave devices on piezoelectric GaAs membranes as thin as 0.5 μm [6]. There are two advantages to this approach [4]. The first is that it is possible to launch acoustic modes in these membranes, specifically, flexural plate waves (FPW) and thickness shear modes (TSM), that will propagate when the sensor is submerged in a liquid. The SAW mode is highly damped in a liquid and does not propagate along the sensor substrate. The second advantage is that the sensitivity to added mass for each of these modes increases with decreasing membrane thickness. Potentially, FPW and TSM acoustic wave chemical sensors can be made much more sensitive than technically realizable SAW sensors.

FPW delay lines are fabricated much the same as SAW delay lines, except that the IDTs are placed on a membrane whose thickness is less than the wavelength of the FPW. Acoustic mode wavelength is determined by the spacing between adjacent IDT fingers for both FPWs and SAWs. Since IDTs are fabricated before the membrane is formed, it is possible to test both SAW and FPW propagation with the same device. An example of this is shown in Fig. 14. Prior to the release etch that forms the membrane, the SAW mode exhibits a peak in its frequency response at 320 MHz. After the release etch, the peak in the frequency response shifts to 220 MHz. This shift to lower frequency is one characteristic of FPW modes and results from the reduced acoustic phase velocity for FPW modes relative to SAW modes.

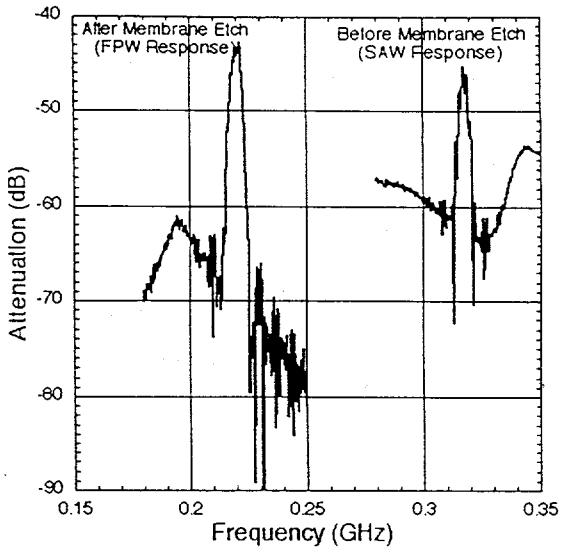

Fig. 14: Comparison of SAW and FPW frequency response. Measurements are taken on the same device before (SAW) and after (FPW) the membrane release etch. The shift to lower frequency is characteristic of the FPW mode, the result of a reduced acoustic phase velocity.

FPW phase velocity scales with t/λ, where t is the membrane thickness and λ is the FPW wavelength. FPW velocity goes to zero for small t/λ and approaches the SAW value in the limit of large t/λ. For a given material, FPW velocity falls on a single curve for all values of t and λ, when plotted against t/λ. This dependence on t/λ is a clear indication of FPW mode propagation. A comparison of FPW phase velocity data to the theoretical prediction is shown in Fig. 15 for several membrane thicknesses. Phase velocity is determined by multiplying the frequency corresponding to the maximum response (as shown in Fig. 14) by the wavelength (determined by the IDT spacing). This is just a restatement of the relationship $v = f\lambda$. The theoretical curve is completely determined by GaAs materials properties. As such, there are no adjustable parameters to fit to the data. As seen in the Fig. 15, the agreement between theory and experiment is excellent. FPW resonators are now being constructed.

It is also possible to create a TSM resonator in the GaAs membrane, where the two surfaces of the membrane act as acoustic "mirrors". For this mode, the resonant frequency is given by $f = 1.67/t$ GHz, where t is measured in microns [8]. This is in good agreement with the measured resonance in 0.5 μm thick GaAs membranes (see Fig. 16). Multiple resonances were observed for 1.0 μm membranes, making identification of the fundamental mode difficult. No resonance was found in the 3.0 μm membranes. Additional study of these devices is underway.

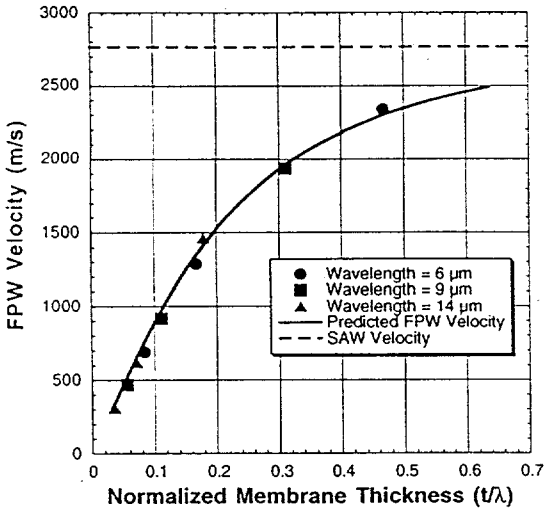

Fig. 15: Comparison between measured FPW phase velocity and theoretical prediction for three membrane thicknesses (0.5, 1.0, and 3.0 μm) and three acoustic wavelengths. No adjustable parameters were used to fit the data.

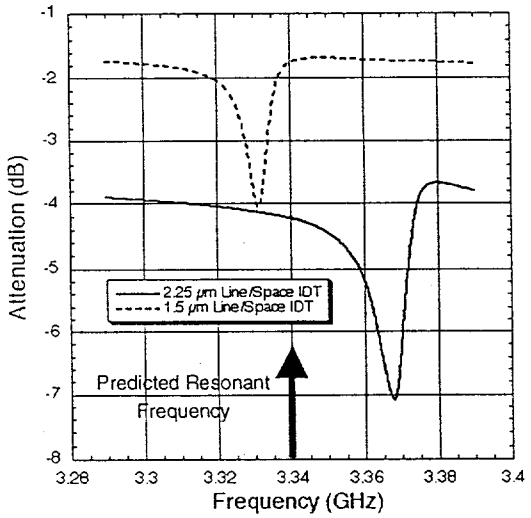

Fig. 16: TSM resonances for two 0.5 μm thick GaAs membranes. Predicted resonant frequency is 3.34 GHz.

6. CONCLUSION

Trace level detection of chemical warfare agent simulants has been accomplished using microfabricated chemical analysis components. A sample concentrator, a gas chromatographic column, and a 4-element surface acoustic wave sensor array have been combined to detect target analytes and interferants with detection limits as low as 10 parts per billion at the system inlet, depending upon the analyte. Pattern recognition algorithms applied to temporally separated detector array responses provide highly reliable identification of a number of analytes. Integration of the detectors with drive and signal conditioning electronics is being explored to improve the performance of high frequency sensors and to simplify packaging. Micromachined acoustic wave devices are being studied because of their potential for greater sensitivity.

7. ACKNOWLEDGEMENTS

Sandia National Laboratories is a multiprogram laboratory operated by Sandia Corporation, a Lockheed Martin Company, for the United States Department of Energy under Contract DE-AC04-94AL85000.

8. REFERENCES

[1] R.P. Manginell et al., "Microfabrication Of Membrane-Based Devices by HARSE and Combined HARSE/Wet Etching", in Proceedings of the SPIE Conference on Micromachining and Microfabrication IV, vol. 3511, 1998, pp. 269-276.

[2] R.P. Manginell et al., "Finite Element Modeling of a Microhotplate for Microfluidic Applications", to be presented at the International Conference on Modeling and Simulation of Microsystems (MSM'99), San Juan, Puerto Rico, April 19-21, 1999.

[3] C.M. Matzke et al., "Microfabricated Silicon Gas Chromatographic Micro-Channels: Fabrication and Performance", in Proceedings of the SPIE Conference on Micromachining and Microfabrication IV, vol. 3511, 1998, pp. 262-268.

[4] D.S. Ballantine et al., Acoustic Wave Sensors: Theory, Design, and Physico-Chemical Applications, San Diego, Academic Press, 1997, ch. 3.

[5] Provided by Jay Grate, Pacific Northwest National Laboratory.

[6] S.A. Casalnuovo et al., "Acoustic Wave Chemical Microsensors in GaAs", in Proceedings of the SPIE Conference on Micromachined Devices and Components IV, vol. 3514, 1998, pp. 103-110.

[7] K. Hjort, "Gallium Arsenide Micromechanics: A Comparison to Silicon and Quartz", Alta Frequenza-Rivista di Elettronica, vol. 6, pp. 48-54, 1994.

[8] J. Soderkvist and K. Hjort, "The Piezoelectric Effect of GaAs Used for Resonators and Resonant Structures", Journal of Micromechanics and Microengineering, vol. 4, 1994, pp. 28-34.